Geophysical Research Letters®

Key Points:

- Biogenic silica diagenesis was examined for the first time in hadal trench sediments
- Availability of detrital materials may be a limiting factor for biogenic silica ($bSiO_2$) diagenesis in $bSiO_2$-rich sediments of the Mariana Trench
- ~40%–80% of dissolved silicic acid generated by $bSiO_2$ dissolution is fixed by authigenic silicate formation

Supporting Information:

Supporting Information may be found in the online version of this article.

Correspondence to:

M. Luo,
mluo@shou.edu.cn

Active Silica Diagenesis in the Deepest Hadal Trench Sediments

Min Luo[1,2] , **Weiding Li[1]**, **Sonja Geilert[3]**, **Andrew W. Dale[3]** , **Zijun Song[1]**, and **Duofu Chen[1]**

[1]Shanghai Engineering Research Center of Hadal Science and Technology, College of Marine Sciences, Shanghai Ocean University, Shanghai, China, [2]Laboratory for Marine Geology, Qingdao National Laboratory for Marine Science and Technology, Qingdao, China, [3]GEOMAR Helmholtz Centre for Ocean Research, Kiel, Germany

Abstract Porewater dissolved silicic acid (DSi) concentrations and stable Si isotope compositions ($\delta^{30}Si$) together with biogenic silica ($bSiO_2$) contents of sediments in five sediment cores collected from the southern Mariana Trench are presented. These data suggest the occurrence of $bSiO_2$ dissolution and concomitant authigenic clay formation in three $bSiO_2$-bearing cores. A reaction-transport model constrained by the measured geochemical data was applied to quantify the rates of Si turnover. Model results predicted the greatest rates of both $bSiO_2$ dissolution and authigenic clay formation at the trench axis core that displayed low $bSiO_2$ contents and abundant detrital materials, suggesting that detrital materials may be a limiting factor for $bSiO_2$ diagenesis. Model results further predicted that ~40%–70% of DSi generated by $bSiO_2$ dissolution is consumed by authigenic clay formation. This is the first study that demonstrates active silica diagenesis in the hadal realm and has implications for understanding benthic Si cycling in deep-sea settings.

Plain Language Summary The marine Si cycle has received extensive attention because it is coupled with the marine carbon cycle, thereby playing a critical role in regulating global climate. While the importance of silica diagenesis in balancing the marine Si cycle has been recognized and studied mostly in estuarine and continental margin environments, very few data exist in deep-sea settings which comprise the majority of the seafloor area. In this study, we aim at understanding the Si cycling in the hadal trench sediments (>6,000 m in water depth) which represent the deepest and least explored sectors of Earth's surface. A reaction-transport model constrained by porewater dissolved silicic acid and stable Si isotope compositions as well as biogenic silica contents from the southern Mariana Trench predicted efficient conversion of biogenic silica to authigenic silicates, which may be controlled by the supply of detrital materials. Our findings provide significant insights into benthic Si and associated elemental cycles in extreme water depths.

1. Introduction

The global silicon (Si) cycle is of great interest as it is closely linked to the global carbon cycle and resulting climatic stability through the coupling of silicate weathering, reverse weathering, and the biological pump (Frings et al., 2016; Sutton et al., 2018; P. J. Tréguer et al., 2021; P. Tréguer & Pondaven, 2000). Silicifying organisms utilize dissolved silicic acid (DSi) in the photic zone of the ocean to build amorphous biogenic silica ($bSiO_2$) frustules. After the death of the organisms, the frustules experience partial dissolution during sinking through the water column because seawater is highly undersaturated with respect to $bSiO_2$. The rapid recycling of $bSiO_2$ to DSi in the water column results in approximately one third of the $bSiO_2$ produced in the photic zone reaching the seafloor (Ragueneau et al., 2000; P. J. Tréguer & Rocha, 2013). Further $bSiO_2$ dissolution can take place in the sediments, leading to <5% of newly synthesized $bSiO_2$ being permanently buried (P. J. Tréguer et al., 2021). Yet, $bSiO_2$ dissolution is often accompanied by the formation of authigenic aluminosilicates (i.e., reverse weathering), thereby potentially involving in atmospheric CO_2 levels over geological timescales (Dunlea et al., 2017; Michalopoulos & Aller, 1995; Rahman et al., 2016). Unraveling the fate of $bSiO_2$ (recycling vs. preservation) in the sediments represents an important component of the marine Si budget, thereby contributing to understanding the cycles of other pertinent elements, such as carbon (Dale et al., 2021). While the importance of silica diagenesis in balancing the marine Si cycle has been recognized and studied mostly in estuarine and continental margin environments, very few data exist in deep-sea settings which comprise the majority of the seafloor area.

Hadal trenches represent the deepest reaches of Earth's surface with water depth over 6,000 m. Growing numbers of in-situ O_2 uptake measurements have shown them to be dynamic hotspots of microbial activity, with generally
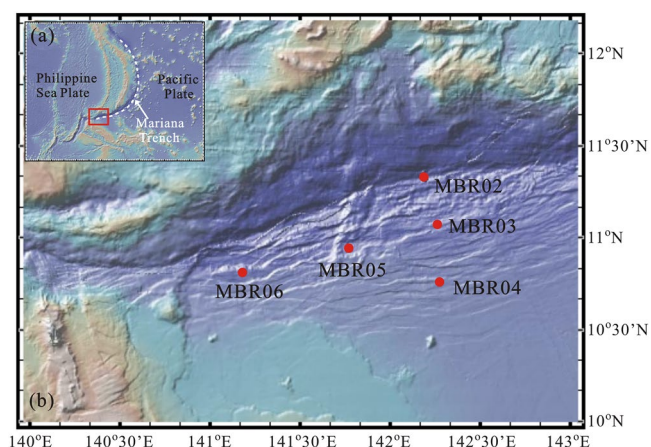
Figure 1. (a) Overview of the study area. (b) Enlargement of the red rectangular in (a) showing the location of the sampling sites.

enhanced but heterogeneous benthic carbon mineralization along the trench axes compared to the abyssal plain (Glud et al., 2013, 2021; Luo, Glud, et al., 2018; Wenzhöfer et al., 2016). These dynamic hotspots are thought to be formed as a result of downslope focusing of relatively labile organic materials triggered by unstable and complex depositional processes within hadal settings (Itou et al., 2000; Oguri et al., 2013; Turnewitsch et al., 2014). The recognition of these unique depositional environments could thus potentially lead to different perceptions on early diagenesis in hadal sediments from the general paradigm based on data in shallower water depths (Jørgensen et al., 2022).

In this study, our objective is to quantitatively examine Si cycling in the southern Mariana Trench sediments. To achieve this, porewater DSi concentrations and stable Si isotope compositions ($\delta^{30}Si$) as well as $bSiO_2$ contents were measured in sediments at five sites with water depths ranging between ~6,000 m and ~10,900 m. Subsequently, the data were simulated using a reaction-transport model to quantify the rates of $bSiO_2$ dissolution and authigenic mineral precipitation. To our knowledge, this study is the first to explore silica diagenesis within hadal depths, and advances our understanding of benthic Si cycling in extreme deep-sea settings.

2. Materials and Methods

2.1. Sampling

The Mariana Trench was formed by the subduction of the Pacific Plate beneath the Philippine Sea Plate, which is famed for hosting the deepest point on the Earth's surface (Challenger Deep) in its southern sector. Sediments and porewater were collected during RV *Tansuoyihao TS15* cruise in 2019. The deepest short core (MBR02) was obtained by pushing a polycarbonate tube into the sediment block retrieved using benthic chambers mounted on an autonomous lander. The other two short cores (MBR05 and MBR06) were retrieved by a box corer. Two longer cores (MBR03 and MBR04) were collected by a gravity corer. Core locations are shown in Figure 1 and Table S1 in Supporting Information S1. Upon recovery, the cores were extruded and sliced into 1–2 cm intervals for porewater collection by inserting Rhizon samplers into the sediment cakes. Aliquots for shore-based DSi and $\delta^{30}Si$ analyses were acidified with HNO_3 (suprapure) and stored in 8 ml Nalgene vials at 4°C.

2.2. Geochemical Analyses of Porewater and Solid Phases

Porewater DSi concentrations were determined by inductively coupled plasma optical emission spectrometry (ICP-OES, ThermoFisher Scientific iCAP 7000). Analytical precision constrained by repeat analysis of spiked IAPSO seawater standard was <3%. Porewater samples for $\delta^{30}Si$ analysis were purified following the method of Georg et al. (2006). The pH of the samples was adjusted to about 2 with concentrated HNO_3. One ml of the diluted samples with a concentration of ~140 μM Si were loaded onto pre-cleaned cation-exchange resins (Biorad AG50 W-X8) and subsequently eluted with 2 ml MQ water. $\delta^{30}Si$ measurements were done on the NeptunePlus HR MC-ICPMS at GEOMAR in medium-resolution mode in 'dry' plasma conditions, using an ESI Apex-HF sample introduction system. The instrumental mass bias was controlled by Mg doping. The blank to signal ratio was ≤0.1%. All samples were measured using the standard-sample bracketing method with the international Si standard NBS28 as the bracketing standard. The reference materials yielded $\delta^{30}Si$ of −1.42 ± 0.11‰ (2SD; $n = 24$) for IRMM018, +1.27 ± 0.12‰ (2SD; n = 68) for Diatomite, and −10.63 ± 0.09‰ (2SD; n = 14) for Big Batch, agreeing well with literature data (e.g., Savage et al., 2010). Additionally, an in-house porewater matrix standard was measured, yielding $\delta^{30}Si$ of 0.93 ± 0.14‰ (2SD; n = 13), comparable within error to the $\delta^{30}Si$ value measured at the NuPlasma MC-ICPMS at GEOMAR (+1.3 ± 0.2‰, 2SD; n = 17; Geilert, Grasse, Doering, et al., 2020; Geilert, Grasse, Wallmann, et al., 2020). The observed offset additionally agreed with the general observation that Si isotopes measured on the Neptune are lower compared to NuPlasma values, though it has not been confirmed yet, if this shift is due to potential instrument biases or the usage of Mg doping regarding isotope

measurements on the Neptune MC-ICPMS (Grasse et al., 2017). Fluid samples were measured at least three times and their δ^{30}Si uncertainties ranged between 0.02 and 0.20‰ (2SD).

Porosity was determined from the weight loss before and after freeze-drying of the wet sediments. The volume fraction of porewater was calculated assuming a dry sediment density of 2.5 g cm^{-3} and a density of the porewater of 1.023 g cm^{-3} ($P = 1$ bar, $T = 25$°C, $S = 35$). bSiO$_2$ was extracted using the method described by Mortlock and Froelich (1989). The contents of bSiO$_2$ were determined following the automatic NaOH leaching method of Müller and Schneider (1993) with a precision of 5%–10%. This classical operationally defined fraction has been shown to underestimate bSiO$_2$ content as diatom frustules coated with authigenic metal oxides and authigenic aluminosilicate converted from bSiO$_2$ dissolution are not extracted (Michalopoulos & Aller, 2004; Rahman et al., 2017). TOC contents were determined by high temperature combustion on a Vario Pyro Cube elemental analyzer after 10% HCl treatment. The analytical precision determined by duplicate measurements was better than 0.03%. The average sedimentation rate for each modeled core can only be estimated from ^{14}C ages of bulk organic carbon as the cores were collected well below the carbonate compensation depth. The radiocarbon contents of sedimentary TOC (Δ^{14}C$_{TOC}$) were determined using AMS at Guangzhou Institute of Geochemistry, Chinese Academy of Sciences. AMS-^{14}C ages were converted to calendar years before present (years B.P, relative to CE 1950) using the Calib.7.1 Program with the IntCal13 calibration curve and the global average reservoir age (∼400 years; Reimer et al., 2013).

2.3. Reaction-Transport Modeling

A one-dimensional reaction-transport model modified from previous studies was applied to simulate Si turnover in the three bSiO$_2$-bearing cores (MBR02, MBR05, and MBR06) (Ehlert et al., 2016; Geilert, Grasse, Doering, et al., 2020; Geilert, Grasse, Wallmann, et al., 2020). The diagenetic reactions considered in the model include bSiO$_2$ dissolution and secondary authigenic aluminosilicate formation, which were mainly constrained by porewater DSi and δ^{30}Si as well as bSiO$_2$ content. Two partial differential equations were used to resolve the depth-concentration profiles of solid (bSiO$_2$) and dissolved species (^{30}Si and Si), respectively (Berner, 1980; Boudreau, 1997):

$$(1 - \Phi)\frac{\partial C_s}{\partial t} = -\frac{\partial\left((1 - \Phi) \cdot v_s \cdot C_s\right)}{\partial x} + (1 - \Phi) \cdot \Sigma R \qquad (1)$$

$$\Phi\frac{\partial C_a}{\partial t} = \frac{\partial\left(\Phi \cdot D_s \cdot \frac{\partial C_a}{\partial x}\right)}{\partial x} - \frac{\partial\left(\Phi \cdot v_p \cdot C_a\right)}{\partial x} + \Phi \cdot \Sigma R \qquad (2)$$

where x (cm) is depth in the sediments, t (yr) is time, Φ (dimensionless) is porosity, C_s (dry wt. %) is the solid content, C_a (mmol cm^{-3}) is the concentration of dissolved species, D_s (cm^2 yr^{-1}) is the molecular diffusion coefficient corrected for tortuosity, v_p (cm yr^{-1}) is the burial velocity of porewater, v_s (cm yr^{-1}) is the burial velocity of solids, and ΣR denotes the sum of the rates of Si diagenetic reactions considered in the model. A non-steady-state modeling approach was applied in order to obtain desirable simulation of observations, whereby bSiO$_2$ rain rates were varied over time. The model parameters and kinetic rate expressions are listed in Tables S2–S5 in Supporting Information S1. A full description of the model can be found in the Supporting Information S1.

3. Results and Discussion

3.1. Evidence for bSiO$_2$ Dissolution and Authigenic Clay Formation

Two distinct types of lithology were observed from the retrieved cores. MBR03 and MBR04 were dominated by brown, homogenous, silty to clayed mud and were in absent of biogenic siliceous debris. In addition to the pelagic lithogenic sediments, light yellowish laminated diatom mats (LDMs) were found almost throughout the core MBR05 and in the interval of ∼8–20 cm in core MBR06 with bSiO$_2$ contents reaching up to ∼60% (Figure S1 in Supporting Information S1). The LDMs were predominantly composed of valve fragments of the giant diatom *Ethmodiscus rex* (*E. rex*) with extremely low abundance of other diatom species and radiolarians (<1%). These giant diatoms, with valve length of >50 μM (up to 2–5 mm), were also reported in the sediments of the Philippine Sea and the southern Mariana Trench (Figure S1 in Supporting Information S1) (Luo et al., 2017, Luo, Algeo, et al., 2018; Xiong et al., 2012). In contrast to MBR05 and MBR06, disseminated valve fragments of *E.*
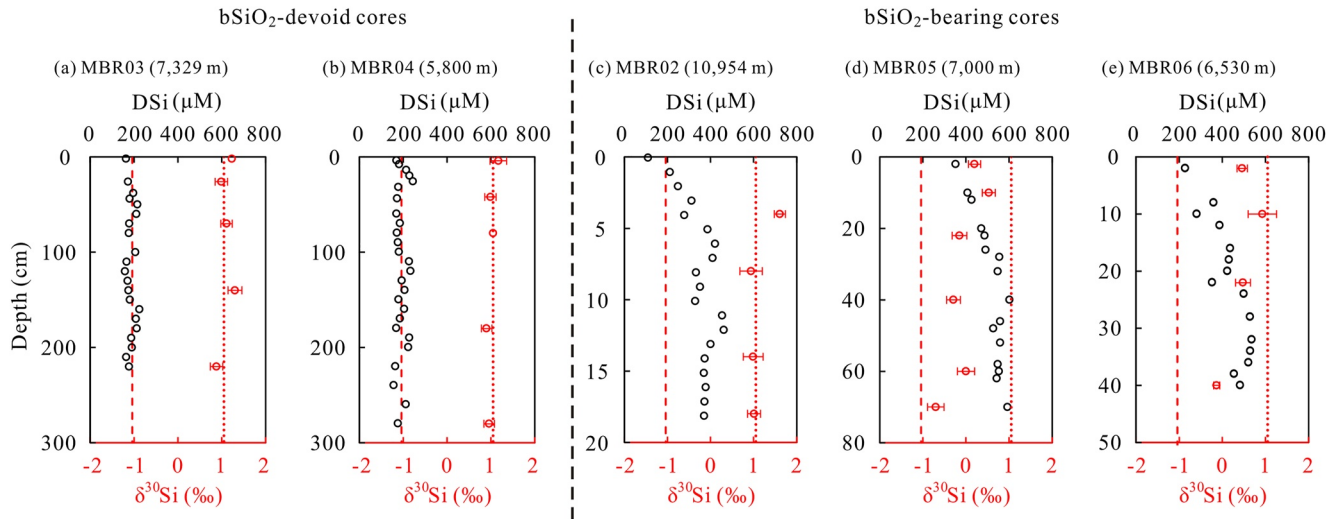
Figure 2. Downcore variations in porewater dissolved silicic acid (DSi) concentrations (black circles) and $\delta^{30}Si$ values (red circles) for biogenic silica (bSiO$_2$)-devoid (a and b) and bSiO$_2$-bearing cores (c, d and e). Red dashed and dotted lines represent $\delta^{30}Si$ values of *E. rex* frustules retrieved from the Philippine Sea basin ($-1.04 \pm 0.22\%$, Xiong et al., 2015) and the western Pacific deep water ($1.05 \pm 0.07\%$, Reynolds et al., 2006), respectively. Error bars for stable Si isotope data are shown except for those data points with error smaller than the symbol size. Note that the downcore trends of porewater DSi and $\delta^{30}Si$ are distinct between bSiO$_2$-bearing (MBR02, MBR05, and MBR06) and bSiO$_2$-devoid (MBR03 and MBR04) cores. Also note the different depth scales.

rex instead of discrete LDM layers were observed in the trench axis core MBR02, with lower bSiO$_2$ contents than in the discrete LDM layers of MBR05 and MBR06. The finding of significantly different sediment compositions in the southern Mariana Trench seems to agree with the assertion that heterogeneity of sediment textures and habitats features the hadal trench environments (Stewart & Jamieson, 2018).

In accordance with the contrast in the sediment bSiO$_2$ contents, porewater DSi concentrations and $\delta^{30}Si$ values showed marked differences in their downcore trends between bSiO$_2$-bearing (MBR02, MBR05, and MBR06) and bSiO$_2$-devoid (MBR03 and MBR04) cores (Figure 2). Porewater DSi concentrations in bSiO$_2$-bearing cores generally increased with depth, reaching quasi-asymptotic values of ~500–600 μM. The DSi concentrations in these cores were much higher than those in bSiO$_2$-devoid cores where no obvious downcore trends were observed. Moreover, porewater $\delta^{30}Si$ values in the bSiO$_2$-bearing cores exhibited noticeable deviation from that of the western Pacific deep water ($1.05 \pm 0.07\%$, Reynolds et al., 2006), whereas porewater $\delta^{30}Si$ values in bSiO$_2$-devoid cores generally displayed seawater-like $\delta^{30}Si$ value throughout the cores (Figure 2).

In bSiO$_2$-bearing cores MBR05 and MBR06, the general downcore increase in porewater DSi concentrations concomitant with lowered $\delta^{30}Si$ values compared to the deep water $\delta^{30}Si$ of western Pacific points to dissolution of *E. rex* frustules given that this dominant mat-forming giant species ($\delta^{30}Si = -1.04 \pm 0.22\%$) is more depleted in ^{30}Si than the small diatoms ($\delta^{30}Si = 1.11 \pm 0.80\%$) (Sutton et al., 2018; Xiong et al., 2015). We surmise that the dissolution of *E. rex* is comparable to that of small diatoms when exposed to an undersaturated environment given their identical chemical composition and *E. rex*'s porous structure. Sensitivity tests of small diatom dissolution on porewater $\delta^{30}Si$ are shown in Figure S2 in Supporting Information S1, which exemplifies the failure of simulating the observations if assuming small diatom dissolution. Similar ^{30}Si-depleted porewater data have been reported for the Guaymas Basin, the Barents Sea, and the Antarctic region, and interpreted as indicators for dissolution of terrigenous clay and metal oxides apart from biogenic opal (Closset et al., 2022; Geilert, Grasse, Doering, et al., 2020; Ward et al., 2022). In the southern Mariana Trench sediments, however, dissolution of lithogenic silicates does not necessarily contribute to the low porewater $\delta^{30}Si$ values because simple dissolution of *E. rex* frustules that represent the predominant diatom species can explain the observations. Indeed, porewater DSi and $\delta^{30}Si$ in bSiO$_2$-devoid cores show no clear indication of lithogenic phases dissolution as they are mainly scattered close to the seawater endmember (Figure 3). Data from the three bSiO$_2$-bearing cores would be expected to plot along the mixing line between deep water and *E. rex* frustule if simple dissolution of bSiO$_2$ was the only process taking place, which is contrary to observations. Rather, porewater $\delta^{30}Si$ values tend to be shifted above the mixing line (Figure 3). The elevated $\delta^{30}Si$ values can be explained by DSi precipitation in the form of
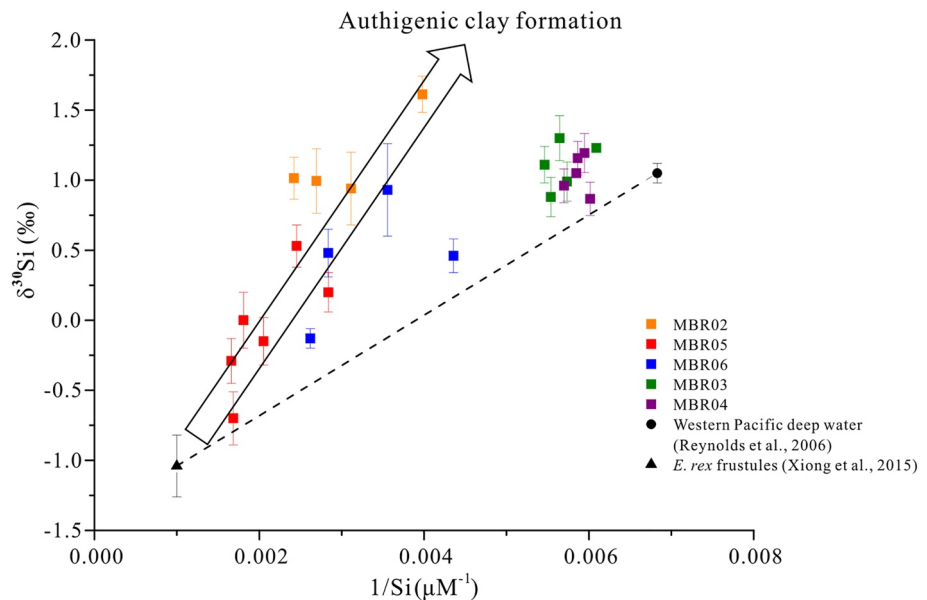
Figure 3. Crossplot of $\delta^{30}Si$ versus 1/Si in porewater. The dashed line represents the two-endmember mixing trend between the western Pacific deep water and *E. rex* frustules. The arrow indicates the potential influence of authigenic clay formation on porewater data. Error bars for stable silicon (Si) isotope data are shown except for those data points with errors smaller than the symbol size. Si concentration for the endmember of *E. rex* frustules was assumed to be the equilibrium concentration in respect to biogenic silica solubility (1000 μM) under the ambient temperature and pressure of the Mariana Trench (Van Cappellen & Qiu, 1997).

authigenic clay minerals following $bSiO_2$ dissolution, given that the lighter Si isotope is preferentially incorporated into the solid phase during low-temperature precipitation reactions (Ehlert et al., 2016; Geilert et al., 2014).

Formation of authigenic aluminosilicate minerals or reverse weathering driven by $bSiO_2$ dissolution has been reported in a variety of marine settings, which represents a potentially important sink for elements (e.g., Mg, K) and alkalinity (Loucaides et al., 2010; Michalopoulos & Aller, 1995, 2004; Michalopoulos et al., 2000; Rahman et al., 2016). However, uptake of K^+ and alkalinity is not observed in MBR02, MBR05, and MBR06 (Figure S3 in Supporting Information S1) where authigenic clay formation is inferred to take place based on porewater $\delta^{30}Si$ data. Given that a variety of authigenic aluminosilicates could form in the sediments, porewater K^+ would not necessarily show a downcore decrease trend if K-poor aluminosilicates (e.g., chlorite and smectite) are the major authigenic products. In addition, alkalinity, on the contrary, exhibits a downcore increasing trend in these three cores (Figure S3 in Supporting Information S1). These typical alkalinity profiles are generated by organic matter mineralization that represents the dominant early diagenetic process in marine sediments, despite the occurrence of reserve weathering (e.g., Wallmann et al., 2008). Therefore, we postulate that porewater $\delta^{30}Si$ could be a more sensitive and straightforward indicator for authigenic clay formation than porewater major element compositions.

3.2. Trends in bSiO₂ Diagenesis

Our model predicts active $bSiO_2$ cycling in the uppermost 10–20 cmbsf, with different rates of $bSiO_2$ dissolution and resulting authigenic clay formation among the three $bSiO_2$-bearing cores (Figure 4 & Table 1). The highest depth-integrated rates of $bSiO_2$ dissolution and authigenic clay formation were found for the trench axis core MBR02. High rates of authigenic clay formation were necessary to reproduce the positive excursion of porewater $\delta^{30}Si$ at 4 cmbsf. Although MBR05 contained the most abundant *E. rex* frustules, with $bSiO_2$ up to 60%, model results revealed significantly muted $bSiO_2$ dissolution and authigenic clay formation (Figure 4). Apart from dissolved silicic acid from $bSiO_2$ dissolution, authigenic clay formation is dependent on the availability of other cations (i.e., Al, K, Fe) in the porewater. In river delta settings where the input of reactive terrigenous materials is substantial, biogenic opal acts as the primary factor limiting the formation of authigenic aluminosilicates (Michalopoulos & Aller, 1995, 2004), whereas in opal-rich sediments, production of authigenic aluminosilicates is mainly regulated by Al and Fe released from reactive lithogenic phases (Ehlert et al., 2016; Loucaides
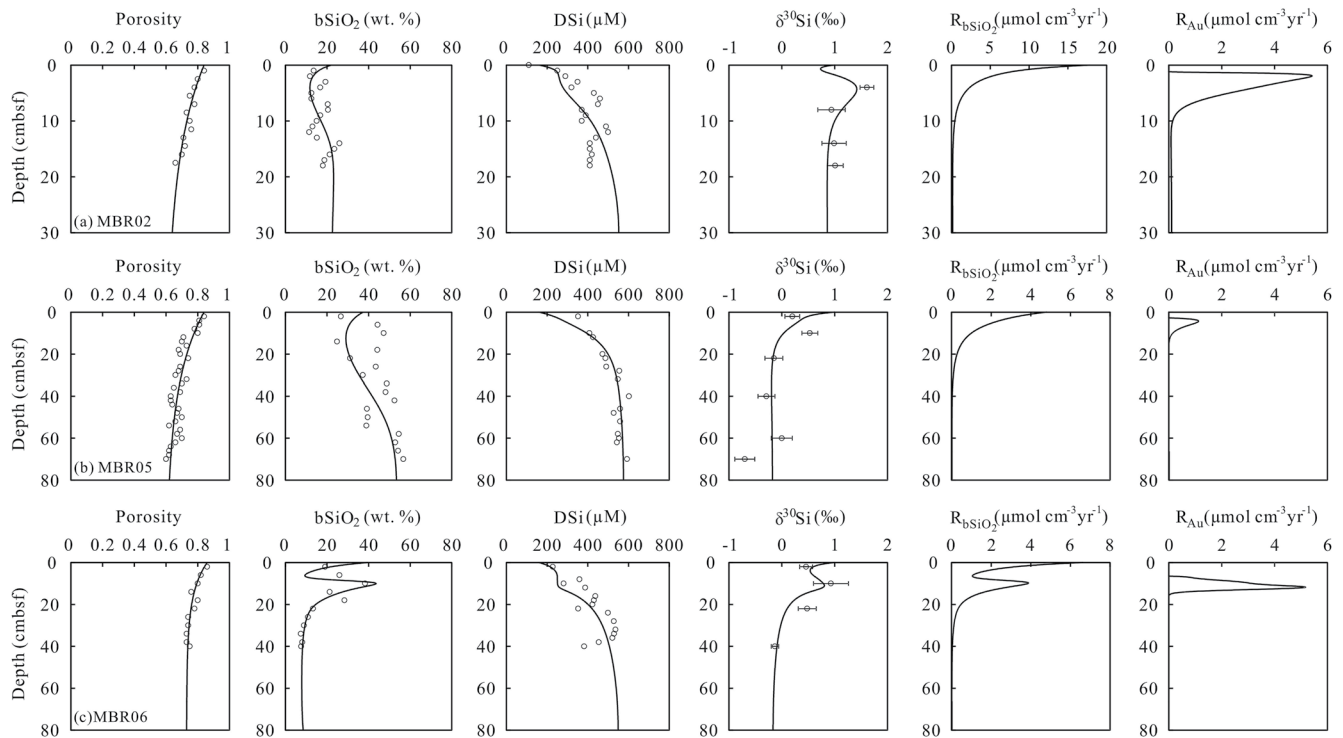
Figure 4. Measured (symbols) and simulated (curves) depth profiles of porosity, biogenic silica (bSiO2), dissolved silicic acid (DSi), and porewater $\delta^{30}Si$, as well as modeled rate profiles of bSiO$_2$ dissolution and authigenic clay precipitation in the bSiO$_2$-bearing cores (MBR02, MBR05, and MBR06). Note the different scales for the rate of bSiO$_2$ dissolution for the three modeled cores.

et al., 2010; Van Cappellen & Qiu, 1997). Therefore, the relatively low Si turnover rates at MBR05 could be explained by limiting amounts of Al and Fe oxide-rich detrital phases, as indicated by lowest detrital fraction at this site compared to the other two bSiO$_2$-bearing cores (Table S6 in Supporting Information S1). The negative correlation between asymptotic DSi values and the ratio of detrital fraction to bSiO$_2$ in a variety of marine environments highlights the potential important role of lithogenic materials in promoting production of secondary authigenic aluminosilicates (Dale et al., 2021; Dixit & Van Cappellen, 2003).

It is noteworthy that a peak in bSiO$_2$ content of ~40% occurs at 10 cmbsf of MBR06, which is accompanied by positive excursion of porewater $\delta^{30}Si$. Based on our model set-up, an elevated bSiO$_2$ content would increase the rate of bSiO$_2$ dissolution, whereby it would be expected that the porewater $\delta^{30}Si$ values would shift to lower values. However, the observation of an opposite trend of $\delta^{30}Si$ variation suggests that authigenic clay formation which preferentially takes up the light Si isotope has a greater impact on the porewater $\delta^{30}Si$ than bSiO$_2$ dissolution

Table 1
Compilation of Silicon (Si) Turnover in Different Marine Environments

Location	bSiO$_2$ dissolution (μmol Si cm^{-2} yr^{-1})	Lithogenic silicate dissolution (μmol Si cm^{-2} yr^{-1})	Authigenic silicate formation (μmol Si cm^{-2} yr^{-1})	Fraction of DSi re-precipitated by authigenic silicate (%)	Dominant lithology
Guaymas Basin[a]	26.4	52.2	7.6	9.7	Siliceous silty clay (14%–22% of bSiO$_2$)
Peruvian margin[b]	234	–	56	24	Diatomaceous mud (4%–12% of bSiO$_2$)
Arctic Barents Sea[c]	5.5–61.7	97.1–490.9	4.7–193.8	3–37	Diatomaceous mud (0.2%–0.4% of bSiO$_2$)
Mariana forearc[d]	-	773.2	776.9	99	Serpentinite mud
Mariana Trench[e]	6.38–28.9	–	2.46–19.1	39–66	Laminated diatom mats/diatomaceous mud (7%–55% of bSiO$_2$)

[a]Geilert, Grasse, Doering, et al. (2020). [b]Ehlert et al. (2016). [c]Ward et al. (2022). [d]Geilert, Grasse, Wallmann, et al. (2020). [e]This study.

representing the source of low $\delta^{30}Si$ value. In order to reproduce the observations, the kinetic constant for authigenic clay precipitation (k_P) at MBR06 was elevated in the interval of 0–15 cm, with a maximum centered at ~8 cm (Table S3 in Supporting Information S1), thereby leading to a substantial increase in the rate of authigenic clay precipitation corresponding to the increase in the rate of $bSiO_2$ dissolution at the same depth (Figure 4). In contrast, the kinetic constants for authigenic clay precipitation at MBR02 and MBR05 were set in synchronization with those for $bSiO_2$ dissolution exhibiting an exponential downcore decrease (Table S3 in Supporting Information S1). As the kinetics of authigenic clay formation in the sediments is poorly constrained, the rate laws assigned in the model can only be viewed as empirical and have no theoretical and experimental basis. Despite the occurrence of LDMs with high $bSiO_2$ contents at 8–20 cmbsf in core MBR06 that were similar to MBR05, model results yielded significantly intensified authigenic clay formation at MBR06. This can be attributed to the differences in the detrital content in both cores, which determines the amount of Al and Fe oxide-bearing phases required to form authigenic aluminosilicates.

Understanding the fate of biogenic opal (recycling vs. burial) in sediments has important implications for evaluating the global Si budget. Rapid recycling of biogenic opal in surface sediments supplies biologically available DSi to the overlying water, which feeds positively back to the growth of planktonic communities. Burial of altered and unaltered $bSiO_2$ represent permanent removal of Si from the ocean reservoir. It has been suggested that total $bSiO_2$ burial could have been substantially underestimated if authigenic clay minerals are unaccounted for; mounting evidence supports the ubiquitous occurrence of authigenic clay formation in sediments (Michalopoulos & Aller, 2004; Rahman et al., 2016, 2017). Our simulations indicate that 39%–66% of DSi released from $bSiO_2$ dissolution is sequestered as authigenic silicates (Table 1). The efficient conversion $bSiO_2$ to authigenic silicates emphasizes the significant contribution of deep-sea sedimentary processes in the oceanic Si sink, in agreement with the quantitative assessments of benthic Si cycling in other marine settings.

4. Conclusions

Porewater DSi and $\delta^{30}Si$ data from five sites in the southern Mariana Trench reflect mixed diagenetic activities of $bSiO_2$ dissolution and authigenic clay formation. Model simulations at three $bSiO_2$-bearing cores reveal highest $bSiO_2$ turnover rates in the trench axis (core MBR02) characterized by the lowest $bSiO_2$ content and highest abundant detrital materials. These results imply that authigenic clay formation in the $bSiO_2$-rich sediments of the Mariana Trench is likely governed by the supply of lithogenic materials. Around 40%–80% of DSi from $bSiO_2$ dissolution is re-precipitated to authigenic aluminosilicates. Our findings have important implications for understanding benthic Si and associated elemental cycles in extreme water depths.

Data Availability Statement

The geochemical data used in the study are available at Mendeley data repository via https://data.mendeley.com/datasets/wdgppdhwcv/1.

References

Berner, R. A. (1980). *Early diagenesis: A theoretical approach*. Princeton University Press.

Boudreau, B. P. (1997). *Diagenetic models and their implementation: Modelling transport and reactions in aquatic sediments*. Springer.

Closset, I., Brzezinski, M. A., Cardinal, D., Dapoigny, A., Jones, J. L., & Robinson, R. S. (2022). A silicon isotopic perspective on the contribution of diagenesis to the sedimentary silicon budget in the Southern Ocean. *Geochimica et Cosmochimica Acta*. https://doi.org/10.1016/j.gca.2022.04.010

Dale, A. W., Paul, K. M., Clemens, D., Scholz, F., Schroller-Lomnitz, U., Wallmann, K., et al. (2021). Recycling and burial of biogenic silica in an open margin oxygen minimum zone. *Global Biogeochemical Cycles*, 35(2), e2020GB006583. https://doi.org/10.1029/2020GB006583

Dixit, S., & Van Cappellen, P. (2003). Predicting benthic fluxes of silicic acid from deep-sea sediments. *Journal of Geophysical Research*, 108(C10), 3334. https://doi.org/10.1029/2002JC001309

Dunlea, A. G., Murray, R. W., Santiago Ramos, D. P., & Higgins, J. A. (2017). Cenozoic global cooling and increased seawater Mg/Ca via reduced reverse weathering. *Nature Communications*, 8(1), 844. https://doi.org/10.1038/s41467-017-00853-5

Ehlert, C., Doering, K., Wallmann, K., Scholz, F., Sommer, S., Grasse, P., et al. (2016). Stable silicon isotope signatures of marine pore waters – Biogenic opal dissolution versus authigenic clay mineral formation. *Geochimica et Cosmochimica Acta*, 191, 102–117. https://doi.org/10.1016/j.gca.2016.07.022

Ehlert, C., Grasse, P., & Frank, M. (2013). Changes in silicate utilisation and upwelling intensity off Peru since the Last Glacial Maximum—insights from silicon and neodymium isotopes. *Quaternary Science Reviews*, 72, 18–35. https://doi.org/10.1016/j.quascirev.2013.04.013

Ehlert, C., Grasse, P., Mollier-Vogel, E., Böschen, T., Franz, J., de Souza, G. F., et al. (2012). Factors controlling the silicon isotope distribution in waters and surface sediments of the Peruvian coastal upwelling. *Geochimica et Cosmochimica Acta*, *99*, 128–145. https://doi.org/10.1016/j.gca.2012.09.038

Frings, P. J., Clymans, W., Fontorbe, G., De La Rocha, C. L., & Conley, D. J. (2016). The continental Si cycle and its impact on the ocean Si isotope budget. *Chemical Geology*, *425*, 12–36. https://doi.org/10.1016/j.chemgeo.2016.01.020

Geilert, S., Grasse, P., Doering, K., Wallmann, K., Ehlert, C., Scholz, F., et al. (2020). Impact of ambient conditions on the Si isotope fractionation in marine pore fluids during early diagenesis. *Biogeosciences*, *17*(7), 1745–1763. https://doi.org/10.5194/bg-17-1745-2020

Geilert, S., Grasse, P., Wallmann, K., Liebetrau, V., & Menzies, C. D. (2020). Serpentine alteration as source of high dissolved silicon and elevated δ30Si values to the marine Si cycle. *Nature Communications*, *11*(1), 5123. https://doi.org/10.1038/s41467-020-18804-y

Geilert, S., Vroon, P. Z., Roerdink, D. L., Van Cappellen, P., & Van Bergen, M. J. (2014). Silicon isotope fractionation during abiotic silica precipitation at low temperatures: Inferences from flow-through experiments. *Geochimica et Cosmochimica Acta*, *142*, 95–114. https://doi.org/10.1016/j.gca.2014.07.003

Georg, R. B., Reynolds, B. C., Frank, M., & Halliday, A. N. (2006). New sample preparation techniques for the determination of Si isotopic compositions using MC-ICPMS. *Chemical Geology*, *235*(1), 95–104. https://doi.org/10.1016/j.chemgeo.2006.06.006

Glud, R. N., Berg, P., Thamdrup, B., Larsen, M., Stewart, H. A., Jamieson, A. J., et al. (2021). Hadal trenches are dynamic hotspots for early diagenesis in the deep sea. *Communications Earth & Environment*, *2*(1), 21. https://doi.org/10.1038/s43247-020-00087-2

Glud, R. N., Wenzhöfer, F., Middelboe, M., Oguri, K., Turnewitsch, R., Canfield, D. E., & Kitazato, H. (2013). High rates of microbial carbon turnover in sediments in the deepest oceanic trench on Earth. *Nature Geoscience*, *6*(4), 284–288. https://doi.org/10.1038/ngeo1773

Grasse, P., Brzezinski, M., Cardinal, D., de Souza, G., Andersson, P., Closset, I., et al. (2017). GEOTRACES intercalibration of the stable silicon isotope composition of dissolved silicic acid in seawater. *Journal of Analytical Atomic Spectrometry*, *32*(3), 562–578. https://doi.org/10.1039/c6ja00302h

Itou, M., Matsumura, I., & Noriki, S. (2000). A large flux of particulate matter in the deep Japan Trench observed just after the 1994 Sanriku-Oki earthquake. *Deep Sea Research Part I: Oceanographic Research Papers*, *47*(10), 1987–1998. https://doi.org/10.1016/s0967-0637(00)00012-1

Jørgensen, B. B., Wenzhöfer, F., Egger, M., & Glud, R. N. (2022). Sediment oxygen consumption: Role in the global marine carbon cycle. *Earth-Science Reviews*, *228*, 103987. https://doi.org/10.1016/j.earscirev.2022.103987

Loucaides, S., Michalopoulos, P., Presti, M., Koning, E., Behrends, T., & Van Cappellen, P. (2010). Seawater-mediated interactions between diatomaceous silica and terrigenous sediments: Results from long-term incubation experiments. *Chemical Geology*, *270*(1), 68–79. https://doi.org/10.1016/j.chemgeo.2009.11.006

Luo, M., Algeo, T. J., Tong, H., Gieskes, J., Chen, L., Shi, X., & Chen, D. (2018). More reducing bottom-water redox conditions during the Last Glacial Maximum in the southern Challenger Deep (Mariana Trench, Western Pacific) driven by enhanced productivity. *Deep Sea Research Part II: Topical Studies in Oceanography*, *155*, 70–82. https://doi.org/10.1016/j.dsr2.2017.01.006

Luo, M., Gieskes, J., Chen, L., Shi, X., & Chen, D. (2017). Provenances, distribution, and accumulation of organic matter in the southern Mariana Trench rim and slope: Implication for carbon cycle and burial in hadal trenches. *Marine Geology*, *386*, 98–106. https://doi.org/10.1016/j.margeo.2017.02.012

Luo, M., Glud, R. N., Pan, B., Wenzhöfer, F., Xu, Y., Lin, G., & Chen, D. (2018). Benthic carbon mineralization in hadal trenches: Insights from in situ determination of benthic oxygen consumption. *Geophysical Research Letters*, *45*(6), 2752–2760. https://doi.org/10.1002/2017gl076232

Michalopoulos, P., & Aller, R. C. (1995). Rapid clay mineral formation in amazon delta sediments: Reverse weathering and oceanic elemental cycles. *Science*, *270*(5236), 614–617. https://doi.org/10.1126/science.270.5236.614

Michalopoulos, P., & Aller, R. C. (2004). Early diagenesis of biogenic silica in the Amazon delta: Alteration, authigenic clay formation, and storage. *Geochimica et Cosmochimica Acta*, *68*(5), 1061–1085. https://doi.org/10.1016/j.gca.2003.07.018

Michalopoulos, P., Aller, R. C., & Reeder, R. J. (2000). Conversion of diatoms to clays during early diagenesis in tropical, continental shelf muds. *Geology*, *28*(12), 1095–1098. https://doi.org/10.1130/0091-7613(2000)028<1095:codtcd>2.3.co;2;2

Mortlock, R. A., & Froelich, P. N. (1989). A simple method for the rapid determination of biogenic opal in pelagic marine sediments. *Deep Sea Research Part A. Oceanographic Research Papers*, *36*(9), 1415–1426.

Müller, P. J., & Schneider, R. (1993). An automated leaching method for the determination of opal in sediments and particulate matter. *Deep Sea Research Part I: Oceanographic Research Papers*, *40*(3), 425–444. https://doi.org/10.1016/0967-0637(93)90140-x

Oguri, K., Kawamura, K., Sakaguchi, A., Toyofuku, T., Kasaya, T., Murayama, M., et al. (2013). Hadal disturbance in the Japan trench induced by the 2011 Tohoku–Oki earthquake. *Scientific Reports*, *3*(1), 1910–1915.

Ragueneau, O., Tréguer, P., Leynaert, A., Anderson, R. F., Brzezinski, M. A., DeMaster, D. J., et al. (2000). A review of the Si cycle in the modern ocean: Recent progress and missing gaps in the application of biogenic opal as a paleoproductivity proxy. *Global and Planetary Change*, *26*(4), 317–365. https://doi.org/10.1016/s0921-8181(00)00052-7

Rahman, S., Aller, R. C., & Cochran, J. K. (2016). Cosmogenic 32Si as a tracer of biogenic silica burial and diagenesis: Major deltaic sinks in the silica cycle. *Geophysical Research Letters*, *43*(13), 7124–7132. https://doi.org/10.1002/2016GL069929

Rahman, S., Aller, R. C., & Cochran, J. K. (2017). The missing silica sink: Revisiting the marine sedimentary Si cycle using Cosmogenic 32Si. *Global Biogeochemical Cycles*, *31*(10), 1559–1578. https://doi.org/10.1002/2017GB005746

Reimer, P. J., Bard, E., Bayliss, A., Beck, J. W., Blackwell, P. G., Bronk Ramsey, C., et al. (2013). IntCal13 and Marine13 radiocarbon age calibration curves 0-50,000 years cal BP. *Radiocarbon*, *55*(4), 1869–1887. https://doi.org/10.2458/azu_js_rc.55.16947

Reynolds, B. C., Frank, M., & Halliday, A. N. (2006). Silicon isotope fractionation during nutrient utilization in the North Pacific. *Earth and Planetary Science Letters*, *244*(1), 431–443. https://doi.org/10.1016/j.epsl.2006.02.002

Savage, P. S., Georg, R. B., Armytage, R. M. G., Williams, H. M., & Halliday, A. N. (2010). Silicon isotope homogeneity in the mantle. *Earth and Planetary Science Letters*, *295*(1), 139–146. https://doi.org/10.1016/j.epsl.2010.03.035

Stewart, H. A., & Jamieson, A. J. (2018). Habitat heterogeneity of hadal trenches: Considerations and implications for future studies. *Progress in Oceanography*, *161*, 47–65. https://doi.org/10.1016/j.pocean.2018.01.007

Sun, X., Andersson, P., Humborg, C., Gustafsson, B., Conley, D. J., Crill, P., & Mörth, C. M. (2011). Climate dependent diatom production is preserved in biogenic Si isotope signatures. *Biogeosciences*, *8*(11), 3491–3499. https://doi.org/10.5194/bg-8-3491-2011

Sutton, J. N., André, L., Cardinal, D., Conley, D. J., de Souza, G. F., Dean, J., et al. (2018). A review of the stable isotope Bio-geochemistry of the global silicon cycle and its associated Trace elements. *Frontiers of Earth Science*, *5*. https://doi.org/10.3389/feart.2017.00112

Tréguer, P., & Pondaven, P. (2000). Silica control of carbon dioxide. *Nature*, *406*(6794), 358–359. https://doi.org/10.1038/35019236

Tréguer, P. J., & Rocha, C. L. D. L. (2013). The world ocean silica cycle. *Annual Review of Marine Science*, *5*(1), 477–501. Retrieved from https://www.annualreviews.org/doi/abs/10.1146/annurev-marine-121211-172346

Tréguer, P. J., Sutton, J. N., Brzezinski, M., Charette, M. A., Devries, T., Dutkiewicz, S., et al. (2021). Reviews and syntheses: The biogeochemical cycle of silicon in the modern ocean. *Biogeosciences*, *18*(4), 1269–1289. https://doi.org/10.5194/bg-18-1269-2021

Turnewitsch, R., Falahat, S., Stehlikova, J., Oguri, K., Glud, R. N., Middelboe, M., et al. (2014). Recent sediment dynamics in hadal trenches: Evidence for the influence of higher-frequency (tidal, near-inertial) fluid dynamics. *Deep Sea Research Part I: Oceanographic Research Papers*, *90*, 125–138. https://doi.org/10.1016/j.dsr.2014.05.005

Van Cappellen, P., & Qiu, L. (1997). Biogenic silica dissolution in sediments of the Southern Ocean. I. Solubility. *Deep Sea Research Part II: Topical Studies in Oceanography*, *44*(5), 1109–1128. https://doi.org/10.1016/s0967-0645(96)00113-0

Wallmann, K., Aloisi, G., Haeckel, M., Tishchenko, P., Pavlova, G., Greinert, J., et al. (2008). Silicate weathering in anoxic marine sediments. *Geochimica et Cosmochimica Acta*, *72*(12), 2895–2918. https://doi.org/10.1016/j.gca.2008.03.026

Ward, J. P. J., Hendry, K. R., Arndt, S., Faust, J. C., Freitas, F. S., Henley, S. F., et al. (2022). Benthic silicon cycling in the Arctic Barents Sea: A reaction-transport model study. *Biogeosciences Discussions*, *2022*, 1–34. Retrieved from https://bg.copernicus.org/preprints/bg-2022-51/

Wenzhöfer, F., Oguri, K., Middelboe, M., Turnewitsch, R., Toyofuku, T., Kitazato, H., & Glud, R. N. (2016). Benthic carbon mineralization in hadal trenches: Assessment by in situ O_2 microprofile measurements. *Deep Sea Research Part I: Oceanographic Research Papers*, *116*, 276–286. https://doi.org/10.1016/j.dsr.2016.08.013

Xiong, Z., Li, T., Algeo, T., Doering, K., Frank, M., Brzezinski, M. A., et al. (2015). The silicon isotope composition of Ethmodiscus rex laminated diatom mats from the tropical West Pacific: Implications for silicate cycling during the Last Glacial Maximum. *Paleoceanography*, *30*(7), 803–823. https://doi.org/10.1002/2015pa002793

Xiong, Z., Li, T., Algeo, T., Nan, Q., Zhai, B., & Lu, B. (2012). Paleoproductivity and paleoredox conditions during late Pleistocene accumulation of laminated diatom mats in the tropical West Pacific. *Chemical Geology*, *334*, 77–91. https://doi.org/10.1016/j.chemgeo.2012.09.044